doi:10.1093/brain/awh331 *Brain* (2005), **128**, 158–173

Microanatomy of the dysplastic neocortex from epileptic patients

L. Alonso-Nanclares,[1] R. Garbelli,[3] R. G. Sola,[2] J. Pastor,[2] L. Tassi,[4] R. Spreafico[3] and J. DeFelipe[1]

[1]*Instituto Cajal, CSIC and* [2]*Departamento de Neurocirugía, Hospital de la Princesa, Madrid, Spain,* [3]*Istituto Nazionale Neurologico 'Carlo Besta' and* [4]*Niguarda Hospital 'C. Munari' Epilepsy Surgery Center, Milano, Italy*

Correspondence to: Javier DeFelipe, Instituto Cajal (CSIC), Ave Doctor Arce, 37, 28002 Madrid, Spain
E-mail: defelipe@cajal.csic.es

Summary

Focal cortical dysplasia (FCD) is a pathology that is characterized by the abnormal development of the neocortex. Indeed, a wide range of abnormalities in the cortical mantle have been associated with this pathology, including cytoarchitectonic alterations and the presence of dysmorphic neurons, balloon cells and ectopic neurons in the white matter. FCD is commonly associated with epilepsy, and hence we have studied the ultrastructure of cortical tissue resected from three subjects with intractable epilepsy secondary to cortical dysplasia to identify possible alterations in synaptic circuitry, using correlative light and electron microscopic methods. While the balloon cells found in this tissue do not appear to receive synaptic contacts, the ectopic neurons in the white matter were abnormally large and were surrounded by hypertrophic basket formations immunoreactive for the calcium-binding protein parvalbumin. Furthermore, these basket formations formed symmetrical (inhibitory) synapses with both the somata and the proximal portion of the dendrites of these giant ectopic neurons. A quantitative analysis revealed that in the dysplastic tissue, the density of excitatory and inhibitory synapses was different from that of the normal adjacent cortex. Both increases and decreases in synaptic density were observed, as well as changes in the proportion of excitatory and inhibitory synapses. However, we could not establish a common pattern of changes, either in the same patients or between different patients. These results suggest that cortical dysplasia leads to multiple changes in excitatory and inhibitory synaptic circuits. We discuss the possible relationship between these alterations and epilepsy, bearing in mind the possible limitations that preclude the extrapolation of the results to the whole population of epileptic patients with dysplastic neocortex.

Keywords: cortical circuits; GABAergic system; parvalbumin; basket cells; electron microscopy

Abbreviations: FCD = focal cortical dysplasia; NeuN = neuron-specific nuclear protein; PV = parvalbumin

Received June 1, 2004. Revised July 26, 2004. Second revision September 30, 2004. Accepted October 4, 2004. Advance Access publication November 17, 2004

Introduction

Symptomatic epilepsy is a common human brain dysfunction that is associated with a wide variety of pathologies (Meldrum and Bruton, 1992; Honavar and Meldrum, 1997; DeFelipe, 1999). Nevertheless, malformations of the cerebral cortex cause ~20% of drug-resistant epilepsies in adults, and ~40% in children (Kuzniecky and Barkovich, 1996). Focal cortical dysplasia (FCD) is a condition in which malformations are produced during the development of the cortex, provoking abnormalities in the laminar cortical architecture, alterations in the morphology of neurons and in the appearance of abnormal cells (Taylor's balloon cells and giant neurons), and gliosis (Palmini *et al*., 1994; Garbelli *et al*., 1999*a*, *b*; Kerfoot *et al*., 1999; for a review see Prayson *et al*., 2002). Epileptic seizures in patients with FCD are common, although their causes still remain unclear.

In analysing the causes of epilepsy, several studies have focused on the morphological and functional alterations of inhibitory circuits in FCD. Using GABAergic markers [immunocytochemistry for the calcium-binding protein parvalbumin (PV)], these studies have revealed various alterations, including a general decrease in labelling and the presence of hypertrophic PV-immunoreactive basket formations around the unlabelled somata of giant neurons (Spreafico *et al*., 1998*a*, 2000; Garbelli *et al*., 1999*a*, *b*). Along similar lines, Avoli and colleagues (2003) proposed that FCD tissue generates synchronous potentials, mainly provoked by

$GABA_A$ receptor-mediated conductance. Similarly, alterations in the excitatory system have also been described, in particular changes in the expression of glutamate receptors (Ying *et al*., 1998; Kerfoot *et al*., 1999; Babb *et al*., 2000; Crino *et al*., 2001).

Through electron microscopy, the cytological characteristics of giant neurons and balloon cells in FCD tissue have been defined, and qualitative information of the synapses in the neuropil has also been obtained (Garbelli *et al*., 1999*a*). However, detailed studies on synaptic circuits are still not available. Therefore, the main aim of this work was to determine what are the principal alterations in the synaptic circuits of epileptic patients with FCD. While most excitatory synapses in the neocortex are formed by glutamatergic axon terminals and are of the asymmetrical type, most inhibitory synapses are formed by GABA-containing axon terminals and are symmetrical (reviewed in White, 1989; Ribak and Roberts, 1990; DeFelipe and Fariñas, 1992; Peters and Palay, 1996). Hence, we compared the overall synaptic density and the types of synapses in different regions of dysplastic tissue with the normal adjacent cortex. In addition, we combined immunocytochemistry for PV with correlative light and electron microscopy, to label certain subpopulations of GABAergic cells that are particularly relevant in epilepsy (DeFelipe, 1999). We paid special attention to the distribution of chandelier cell axon terminals and perisomatic synaptic inputs to giant neurons and balloon cells.

Material and methods

Human brain tissue was obtained from two sources: the Claudio Munari Surgical Center for Epilepsy (Milan, Italy) and Neurosurgery Department, Hospital de la Princesa (Madrid, Spain). Samples from three epileptic patients affected by FCD (Mun34, Mun36 and H175) were obtained after surgical resection. Control brain samples of normal temporal cortex were obtained from epileptic patients with hippocampal sclerosis (three male individuals, H38, H60 and H94: 24, 37 and 27 years old, respectively). Some of this material has been used in previous studies (Marco and DeFelipe, 1997; DeFelipe *et al*., 2002). Surgery was performed only after the patient or parent had given informed consent, according to the Declaration of Helsinki. The institutional ethical committees of both hospitals approved the surgical protocols and those for the use of human tissue. In all cases, MRI studies were performed and abnormal results were detected (Fig. 1) in all patients except one (H175). Some of the clinical details of the patients examined are summarized in Table 1.

Upon removal, the resected brain tissue was immediately fixed in cold 4% paraformaldehyde in phosphate buffer 0.1 M, pH 7.4 (PB). After 2 h, the tissue was cut into small blocks ($\sim 1 \times 1 \times 1$ cm) and was post-fixed in the same fixative for 24–48 h at 4°C. Coronal sections (100 μm) were cut with a Vibratome and collected in series in PB. Some sections were Nissl stained to reveal the laminar boundaries and to study the cytoarchitectonic alterations.

Immunohistochemistry

Free-floating sections were pre-treated in 1% H_2O_2 for 30 min to remove endogenous peroxidase activity, and then for 1 h in PB with 0.25% Triton-X and 3% normal goat or horse serum (for polyclonal antisera and monoclonal antibodies, respectively; Vector Laboratories Inc., Burlingame, CA). The sections were then incubated overnight at 4°C with either mouse anti-PV antibodies (1 : 4000; Swant, Bellinzona, Switzerland) or mouse anti-neuron-specific nuclear protein (NeuN) (1 : 2000; Chemicon, Temecula, CA) and rabbit anti-PV (1 : 4000; Swant). The following day, the sections were rinsed and incubated for 1 h in biotinylated goat anti-rabbit or horse anti-mouse IgG (1 : 200; Vector), then for 30 min in a Vectastain ABC immunoperoxidase kit (Vector) and finally with the chromogen 3,3′ diaminobenzidine tetrahydrochloride (DAB; Sigma-Aldrich, St Louis, MO). After staining, the sections were dehydrated, cleared with xylene and coverslipped.

Fluorescence immunohistochemistry

For immunofluorescence, sections were double stained for NeuN and PV, using the same primary antibodies, dilutions and incubation

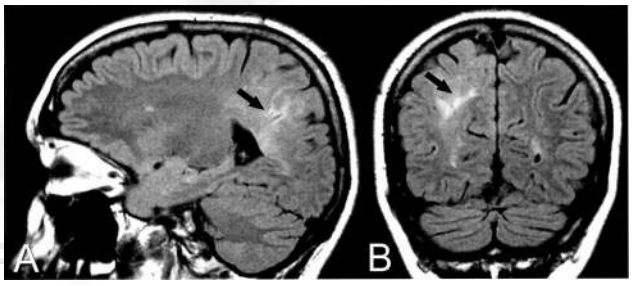

Fig. 1 MRI from patient Mun34, showing a lesioned area (arrows) in the right parietal lobe corresponding to Taylor's type FCD. (**A**) Sagittal plane and (**B**) coronal plane.

Table 1 *Classification of cases, lesion localization and clinical characteristics*

Patient	Age (years), sex, side	Age of onset, duration (years)	Lesion location	Seizure frequency	MRI	Engel scale (time after surgery, in months)
Mun34	24, F, R	16, 8	Parietal lobe	1/week	Hypersignal in grey and white matter, with blurring in parietal region	III (48)
Mun36	3.5, F, L	1, 2.5	Fronto-insular	>1/week	Hypersignal in grey and white matter in frontal region	I (48)
H175	24, M, R	2, 22	Inferior frontal gyrus (Broca's region)	1–5/day	Normal	III (24)

M = male; F = female; R = right; L = left. Engel scale for surgical outcome (Engel, 1987) = class I, seizure-free; class II, rare seizures; class III, worthwhile improvement.

times as indicated above. Free-floating sections were incubated in a solution containing the primary antibodies (anti-NeuN and anti-PV) and then for 2 h at room temperature in a mixture of a goat anti-rabbit antibody coupled to Alexa 594 (1 : 1000, Molecular Probes, Eugene, OR) and a biotinylated horse anti-mouse IgG (1 : 200, Vector). After rinsing in PB, the sections were incubated for 2 h at room temperature in streptavidin coupled to Alexa fluor 488 (1 : 1000; Molecular Probes), washed and mounted in 50% glycerol in PB.

Sections were examined on a Leica TCS 4D confocal laser-scanning system equipped with an argon/krypton mixed gas laser with excitation peaks at 498 and 649 nm, and attached to a Leitz DMRIB microscope. The fluorescence of Alexa 488 and Alexa 594 was recorded through separate channels. Z-sections at 1.5–2 μm intervals were recorded, and optical stacks of 3–10 images were used for the figures.

For all immunocytochemical procedures, controls consisted of processing selected sections either after replacing the primary antibody with pre-immune goat or horse serum, after omission of the secondary antibody, or after replacement of the secondary antibody with an inappropriate secondary antibody. No significant staining was detected under these control conditions.

Electron microscopy

Sections adjacent to those used for histopathological assessment and some sections immunostained for PV were processed for electron microscopy. These sections were post-fixed in 2% glutaraldehyde in PB for 1 h, treated in 1% osmium tetroxide, dehydrated and flat-embedded in Araldite resin. Plastic-embedded sections were studied by a correlative light and electron microscopic method described in detail elsewhere (DeFelipe and Fairén, 1993). Briefly, sections were photographed under the light microscope and then serially cut into semi-thin (2 μm thick) sections with a Reichert ultramicrotome. The semi-thin sections were stained with 1% toluidine blue in 1% borax, examined under the light microscope, and photographed to locate the area of interest. Selected semi-thin sections were resectioned into serial ultrathin sections having a silver grey interference colour, which correspond to a thickness of ∼60–70 nm (Peachey, 1958). The ultrathin sections were collected on formvar-coated, single-slot grids, stained with uranyl acetate and lead citrate, and examined with a JEOL 1200 EX electron microscope (JEOL USA, Inc., MA). Photographs (×10 000) were printed at a final magnification of ×30 000. The number of synapses per volume was estimated using the size-frequency method (DeFelipe *et al*., 1999). The cross-sectional length of synaptic contacts was measured using a digitizing tablet (Summasketch III, Summagraphics, Seymour, USA) and the Scion Image analysis program (Version beta 4.0.2, NIH Image, Scion Corporation USA, 2000).

Neuronal density was estimated using optical disectors as described by West and Gundersen (1990; see also Williams and Rakic, 1988). Twenty-five optical disectors from each cortical region were analysed per case, in 100 μm Nissl-stained sections adjacent to those used for counting synapses. Optical disectors were made using an oil immersion ×100 objective on a surface of 1596 μm^2 and with a depth of 40 μm, which rendered a study volume of 64 134 μm^3 per optical disector. Nucleoli were counted to obtain an estimate of the number of neurons.

Tissue processing for electron microscopy produced greater tissue shrinkage than Nissl staining. In order to obtain homogeneous estimations of the density of neurons and synapses, this difference in shrinkage was evaluated by measuring the cortical surface in adjacent sections processed for electron microscopy and Nissl staining, using Scion Image analysis (Scion Corporation, Frederick, MD). As a result, cortical tissue was estimated to have shrunk 32.8% when processed for electron microscopy. The number of synapses per neuron in each cortical region studied was obtained by dividing the density of the synapses by the density of neurons for each cortical region after correcting for shrinkage. Data analysis was performed with the aid of the SPSS statistical package (SPSS Science, Chicago, IL).

Results

Histopathological findings

Consistent with earlier observations, in cortical tissue from patients suffering from FCD, we generally observed disruptions in lamination and gliosis, as well as the presence of abnormal cell types (e.g. giant cells and balloon cells) and ectopic neurons (Spreafico *et al*., 1998*a*, *b*; Garbelli *et al*., 1999*a*,*b*; Tassi *et al*., 2002). The patients were classified according to the criteria defined by Tassi *et al*. (2002). They were all considered within the subgroup of Taylor-type cortical dysplasia, which is characterized histologically by abnormal cortical lamination associated with the presence of ectopic neurons in white matter, giant and dysmorphic neurons and occasional balloon cells (Taylor *et al*., 1971). These balloon cells were readily identified by their large size and rounded shape, and by the ill-defined cell membrane, pale eosinophilic cytoplasm and one or more eccentric nucleoli. Giant neurons were recognized by their abnormally large size despite having a normal appearance, when compared with neighbouring neurons.

The cytoarchitectural alterations displayed by tissue from these patients were not uniform either between patients or within different regions of a given patient. Two distinct histological regions could be identified in the tissue from patients Mun36 and H175, a normal-looking region (Fig. 2A and D) and another region that was clearly malformed (Fig. 2B and E). In the most deformed region of patient Mun36, no cortical layers other than layer I could be recognized, and an intense gliosis could be seen. Nissl staining revealed the presence of balloon cells (Fig. 2C and F) or Taylor's cells (Taylor *et al*., 1971). Giant neurons in the grey and white matter were also detected (Fig. 2B and E). In the tissue from patient H175, a region in which the normal lamination was partially preserved was also observed, but numerous giant neurons (some with inverted orientation) were present throughout the resected neocortex. Cortical tissue from patient Mun34 showed some similar alterations in terms of the abnormal lamination (only layer I could be recognized), and both balloon cells and numerous giant neurons were present, scattered throughout the neocortex.

Immunocytochemical studies

The possible alterations of the GABAergic circuits in these patients were investigated by analysing the distribution of PV immunocytochemistry. In the normal human neocortex,

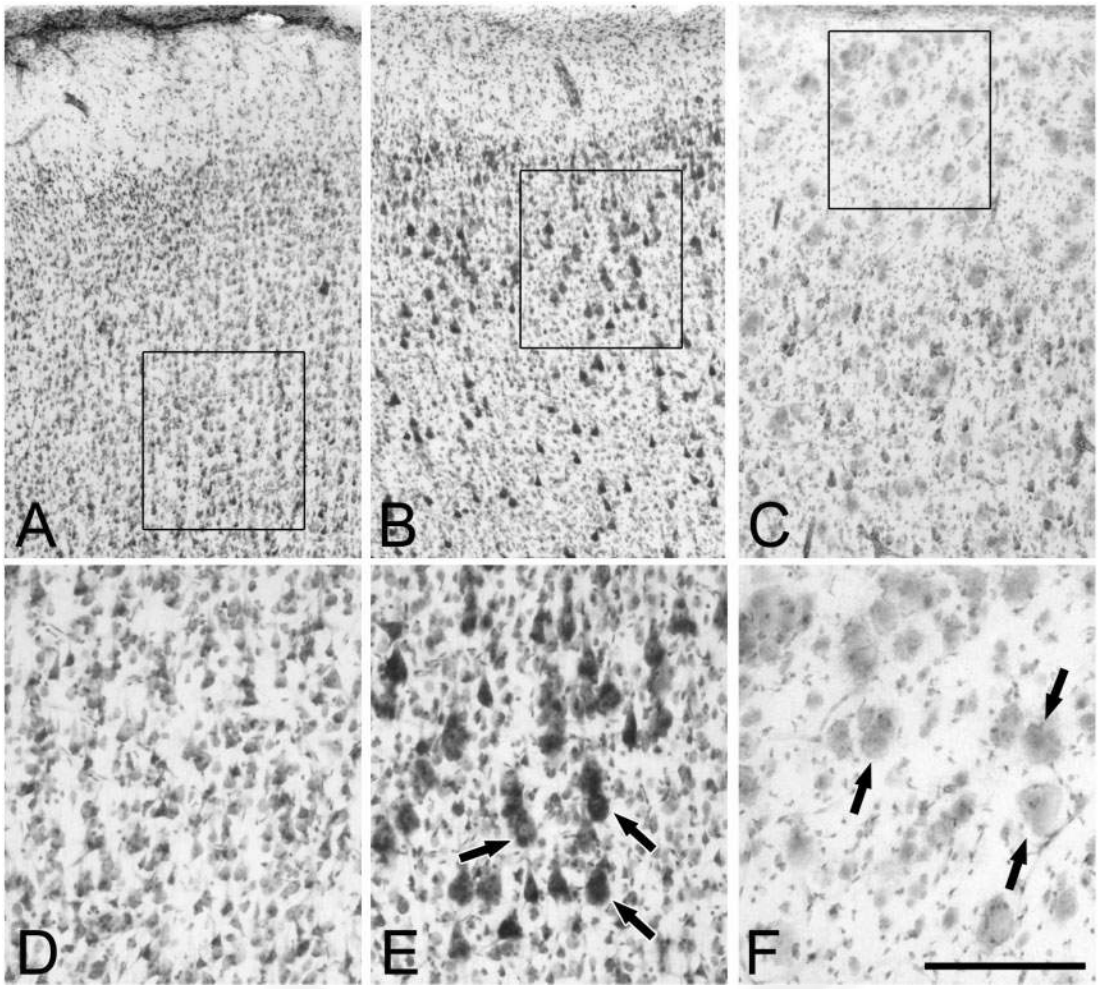

Fig. 2 (**A**–**C**) Low-power photomicrographs of Nissl-stained sections showing the cytoarchitecture of the neocortex from FCD tissue. (**D**–**F**) High-power images of the boxed areas in **A**–**C**. (**A** and **D**) A normal-looking region from the neocortex of patient H175. (**B** and **E**) Altered region from patient H175 adjacent to the region illustrated in **A** and **D**, showing the disruption of the laminar organization and numerous giant pyramidal cells, some of them indicated with arrows. (**C** and **F**) Altered region from patient Mun36, showing balloon cells in the upper layers and an abnormal lamination. Balloon cells (arrows) are large and slightly Nissl stained. Scale bar (in **F**) 470 μm in **A**–**C**, 180 μm in **D**–**F**.

PV labelling is characterized by the staining of numerous non-pyramidal cells, boutons through layers II–VI, and chandelier cell axon terminals (short vertical rows of boutons). In addition, pyramidal cells typically were surrounded by PV-immunoreactive boutons that represent the axon terminals of basket cells (Hendry *et al*., 1989; DeFelipe *et al*., 1989, 1993; del Río and DeFelipe, 1994).

The pattern of PV immunostaining was modified in a variety of ways in FCD tissue, generally reflecting the cytoarchitectonic alterations (Garbelli *et al*., 1999*a*). Few PV-immunoreactive chandelier terminals were observed in the tissue from patient Mun34, although numerous PV-immunoreactive processes (forming small clusters in some regions) and large cell bodies were seen. In some regions of the tissue from patient Mun36, a normal distribution of PV was detected, whereas in other regions staining for PV was considerably reduced in all the neocortical layers. Finally, tissue from patient H175 showed a normal distribution of PV immunoreactivity in some regions, but in others PV immunoreactivity was decreased in chandelier terminals in layer VI. In these latter regions and in the adjacent white matter, abnormal PV-immunoreactive basket formations were present around unlabelled cell bodies and the proximal processes of giant neurons (Fig. 3). These abnormal basket formations were also found in the other two cases.

Double immunofluorescence studies: basket formations in the white matter

In normal cortical tissue, relatively few neurons were found in the white matter and they were labelled for NeuN. In these sections, no PV-immunoreactive neurons were seen and very few PV-immunoreactive terminals were observed (Fig. 4A–C). In the white matter of patient H175, numerous NeuN-immunoreactive giant neurons and hypertrophic PV-immunoreactive basket formations were detected

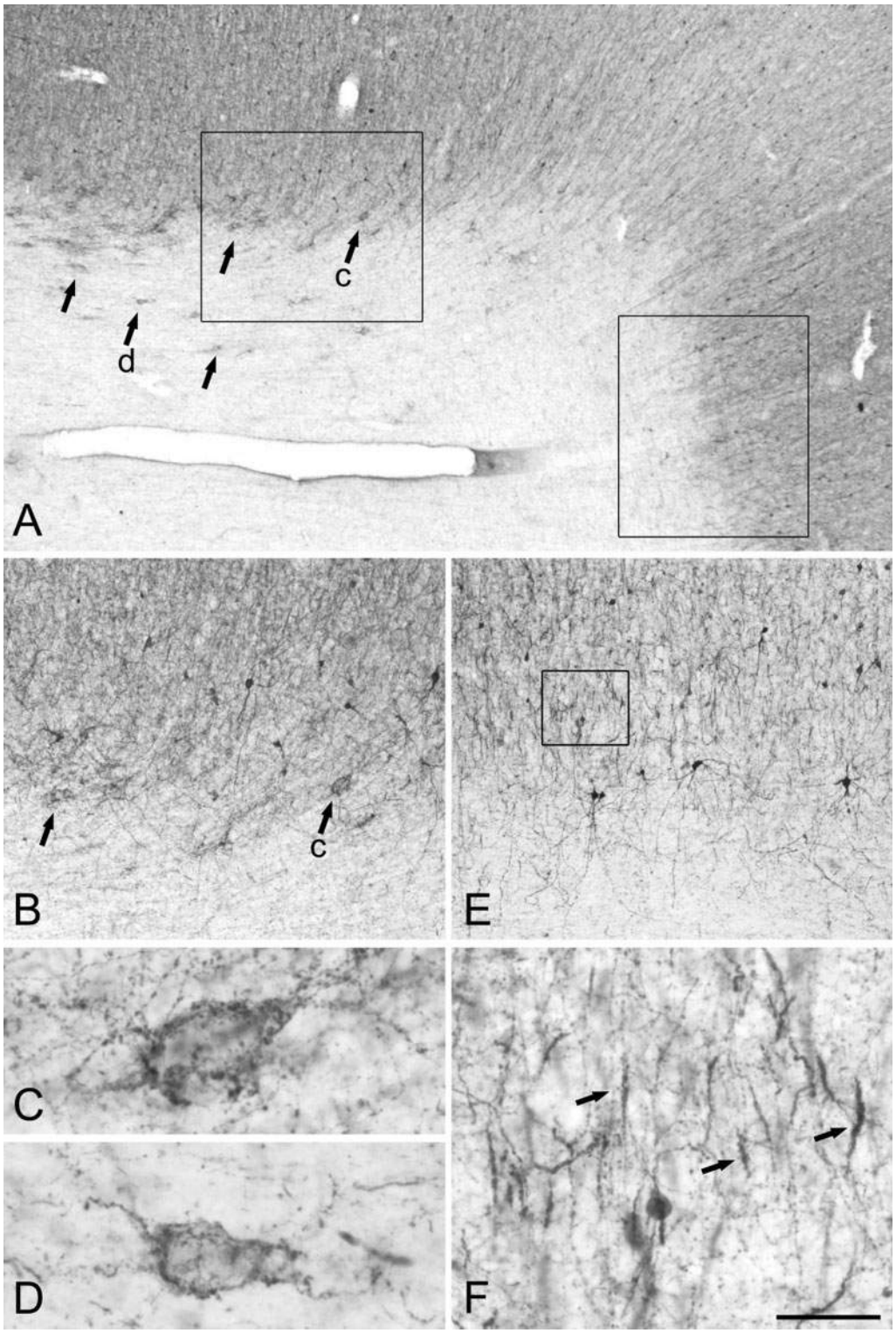

Fig. 3 (**A**) Low-power photomicrograph from a PV-immunostained section of a cortical gyrus from patient H175, showing a region with an abnormal distribution of PV (left) and the adjacent normal regions (right). In the abnormal region, there were hypertrophic basket formations in the grey and white matter (arrows). (**B** and **E**) Higher magnification of the boxed areas in **A** (left and right, respectively). In **B**, note the lack of chandelier axon terminals and the presence of PV-immunoreactive hypertrophic basket formations (arrows) located at the junction of layer VI and the white matter. (**C** and **D**) High-power photomicrograph of the hypertrophic basket formations (c and d) shown in **A**. (**E** and **F**) The normal distribution of PV with numerous PV-immunoreactive chandelier axon terminals (arrows). **F** is a higher magnification of the boxed area in **E**. Scale bar (in **F**) 580 μm in **A**, 270 μm in **B** and **C**, 40 μm in **D** and **E**, and 50 μm in **F**.

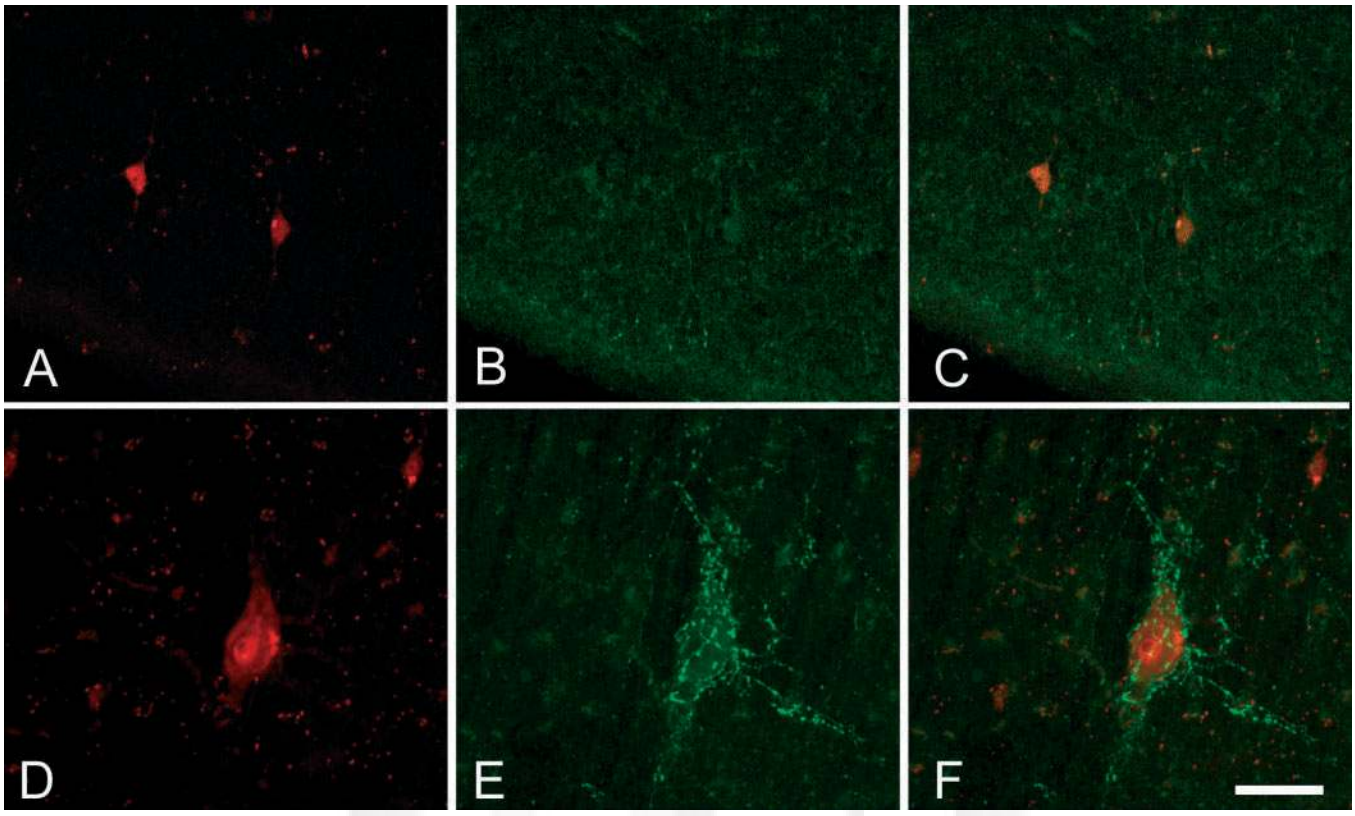

Fig. 4 Series of confocal images of the white matter from control (**A**–**C**) and FCD (**D**–**F**) tissue sections from patient H175, double labelled for NeuN (red) and PV (green). In the normal white matter, neurons are small (**A**) and are not innervated by PV-immunoreactive axon terminals (**B** and **C**). In the white matter of the abnormal regions, there were giant NeuN-immunoreactive neurons (**D**) innervated by hypertrophic basket formations (**E** and **F**). (**A**–**C**) A stack of 10 optical images separated by 2 μm in the *z*-axis (total, 18 μm). (**D**–**F**) A stack of four optical images separated by 1.96 μm in the *z*-axis (total, 6 μm). Scale bar (in **F**) 50 μm in **A**–**F**.

(Fig. 4D and E, see also Fig. 3A and B). To study the relationship between these PV-immunoreactive basket formations and the giant cells in the white matter, we used double labelling immunofluorescence histochemistry. In sections stained for both NeuN and PV, all the giant NeuN-immunoreactive neurons found in the white matter were surrounded by hypertrophic basket formations and all the basket formations were confirmed to be around neurons (Fig. 4D and F; $n = 16$). Since no PV-immunoreactive cell bodies were found in the white matter, these basket formations probably originated from PV-immunoreactive interneurons located in the adjacent grey matter.

Ultrastructural analysis

Of the two major morphological types of cortical synapses, denominated type I and type II by Gray (1959), and that correspond to the asymmetrical and symmetrical types of Colonnier (1968), respectively, both were clearly identified in the tissues analysed (Figs 5A and 6A). For our purposes, synapses having a prominent postsynaptic density (40–50 nm in thickness) were identified as asymmetrical, whereas those with a thinner postsynaptic density (∼20 nm in thickness) were considered as symmetrical (Gray, 1959; Colonnier, 1968, 1981; Peters, 1987; White, 1989; Peters *et al*., 1991; Peters and Palay, 1996). Furthermore, for quantitative analyses, we also considered those synapses in which the synaptic cleft and associated membrane densities could not be visualized clearly (due to the oblique plane of section) as uncharacterized synapses, since they could be classified as neither asymmetrical nor symmetrical (Figs 5A and 6A).

Neuropil

While the ultrastructure of the neuropil from the normal-looking regions of all patients was normal (Peters *et al*., 1991), a variety of alterations were detected in the deformed areas, although sometimes only at certain levels. In these altered regions, the neuropil showed distinct degrees of gliosis with a variable number of glial processes. For example, whereas in the middle levels of the neocortex from patient Mun34, the neuropil appeared normal (Fig. 5A), numerous glial processes were detected in the superficial layers (Fig. 5B). However, the altered regions of the tissue from patient Mun36 showed numerous glial processes in all layers (Fig. 6B) whereas, in contrast, the neuropil of the altered regions of the tissue from patient H175 had a relatively normal aspect with few glial processes.

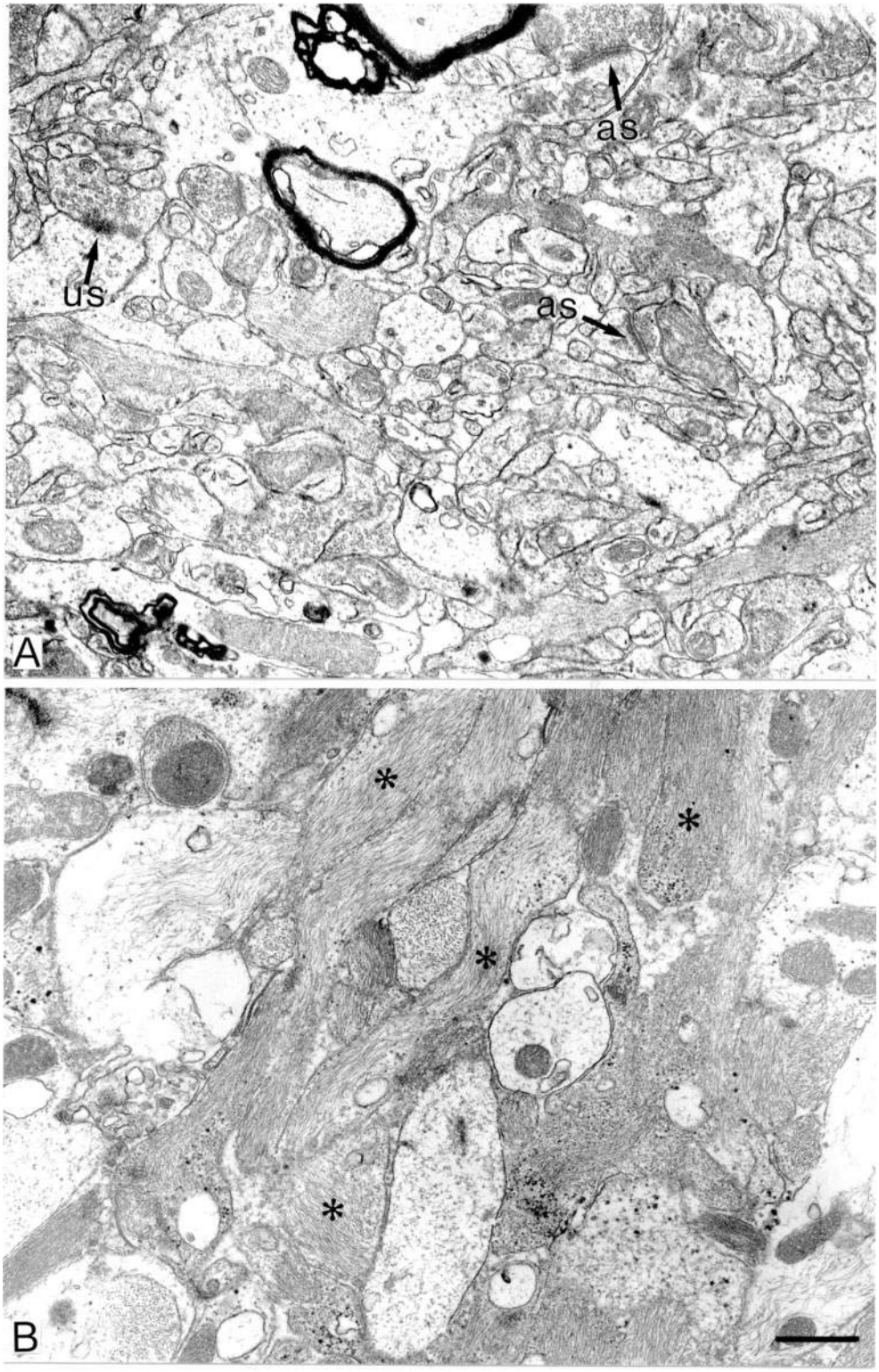

Fig. 5 Electron micrographs of the neuropil from the neocortex of patient Mun34. (**A**) Normal appearance of the neuropil in the deeper layer, showing synaptic contacts, some of which are indicated by arrows. (**B**) Altered neuropil from layer I. Note the lack of synaptic contacts and the presence of numerous glial processes, some of them labelled with asterisks. as = asymmetrical synapse; us = uncharacterized synapse. Scale bar (in **B**) 0.5 μm in **A** and **B**.

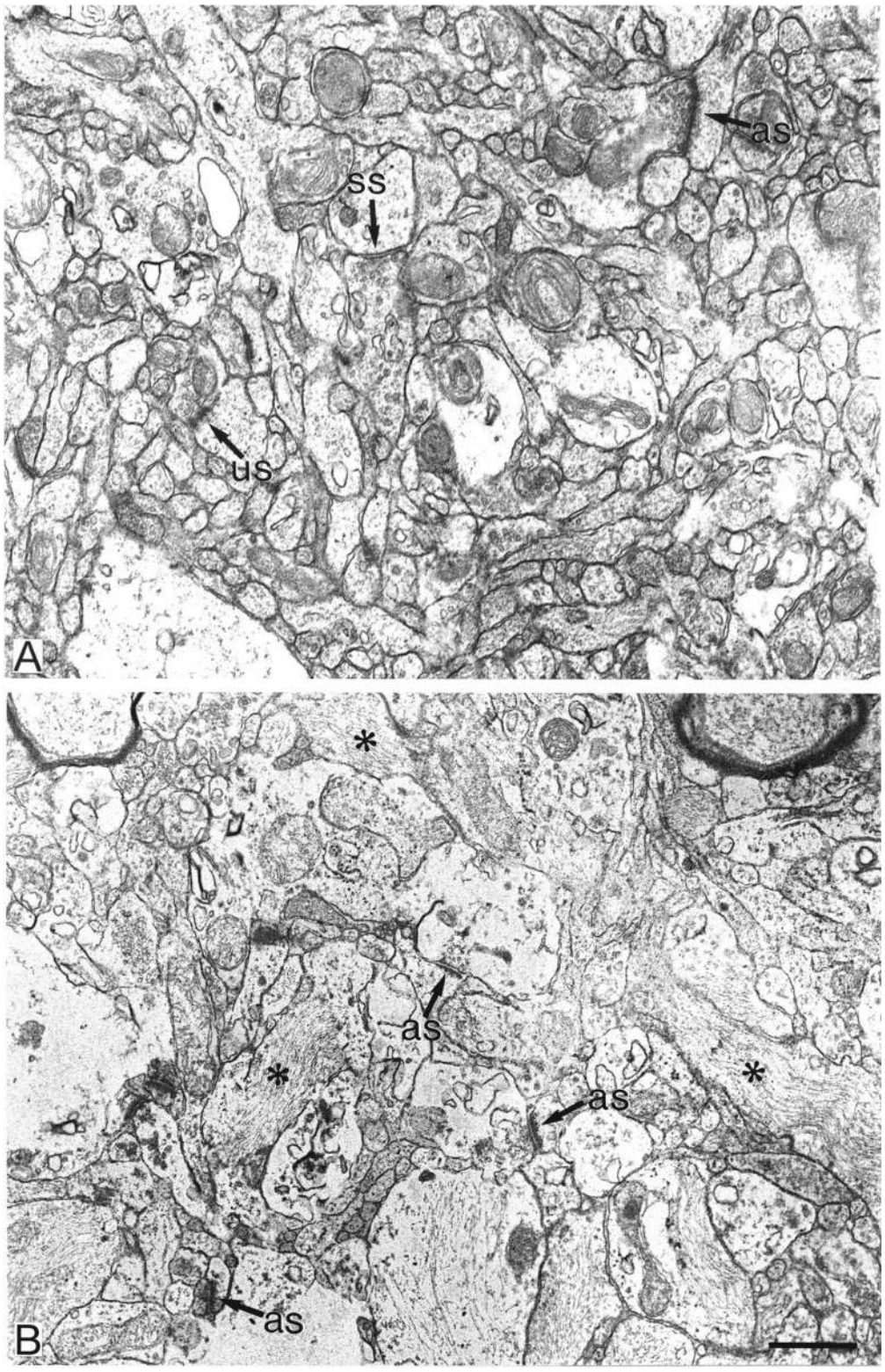

Fig. 6 Electron micrograph of the neuropil from the normal (**A**) and altered (**B**) neocortex of patient Mun36. (**A**) Normal appearance of the neuropil with synaptic contacts, some of which are indicated by arrows. (**B**) In the abnormal neuropil, there are numerous glial processes, some labelled with asterisks. In this abnormal region, there were numerous synapses of the asymmetrical type. as = asymmetrical synapse; ss = symmetrical synapse; us = uncharacterized synapse. Scale bar (in **B**) 0.5 μm in **A** and **B**.

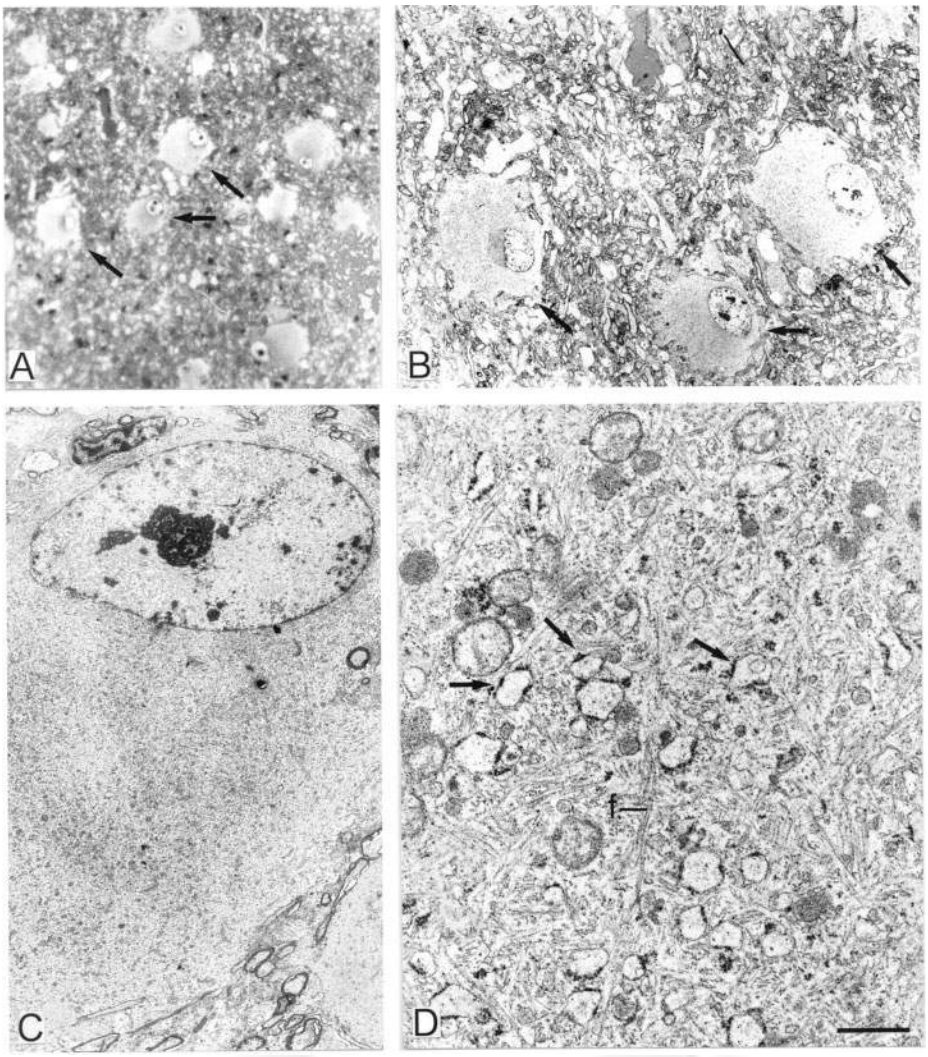

Fig. 7 (**A**) Photomicrograph of a 2 μm thick semi-thin plastic section counterstained with toluidine blue showing several balloon cells (arrows). (**B**) Low-power electron micrograph taken after resection of the semi-thin section shown in **A**. Arrows indicated the same balloon cells as in **A**. (**C**) Higher magnification of a balloon cell, illustrating its perykarion and nucleus. (**D**) Higher magnification of **C**; note the presence of hypertrophic endoplasmic reticulum (arrows) and numerous intermediate filaments (f). Scale bar (in **D**) 70 μm in **A**, 20 μm in **B**, 0.5 μm in **C** and 0.4 μm in **D**.

Balloon and giant cells

In material prepared for electron microscopy, a total of 10 balloon cells and 12 giant neurons were first identified by light microscopy according to the cytological criteria mentioned above. This material was examined using correlative light and electron microscopy. In brief, this consisted of cutting the tissue into 2 μm serial plastic semi-thin sections, and then obtaining serial ultrathin sections from the selected semi-thin sections for analysis at the electron microscope level (Figs 7A and B, and 8A and B). As previously described (Garbelli *et al*., 1999*a*), the cytoplasm of balloon cells is filled with hypertrophic endoplasmic reticulum as well as numerous intermediate filaments, and they contain one or more eccentric nucleoli (Fig. 7). We examined the surface of these cells to see whether they form synapses, but could not identify any axosomatic synapses. In contrast, the giant pyramidal cells showed an apparently normal complement of cytoplasmic organelles (Fig. 8) similar to the typical pyramidal cells (Feldman, 1984). Furthermore, as with pyramidal neurons in the normal neocortex, only axon terminals forming symmetrical synapses were seen to innervate their perisomatic region and the proximal parts of their dendrites (Fig. 8C; see Alonso-Nanclares *et al*., 2004; and references therein).

In addition, we studied the giant neurons that were located in the white matter (some of them identified as pyramidal neurons) and that were surrounded by hypertrophic basket PV-immunoreactive formations (Fig. 9A and B; $n = 9$). These PV-immunoreactive boutons formed symmetrical synapses with the soma of these giant cells (Fig. 9C). However, since the immunostaining of the axon terminal partially masked the postsynaptic density, it was often difficult to identify the nature of the contacts (Fig. 9C). Therefore, no attempt was made to estimate the proportion of PV-immunoreactive boutons forming axosomatic synapses with

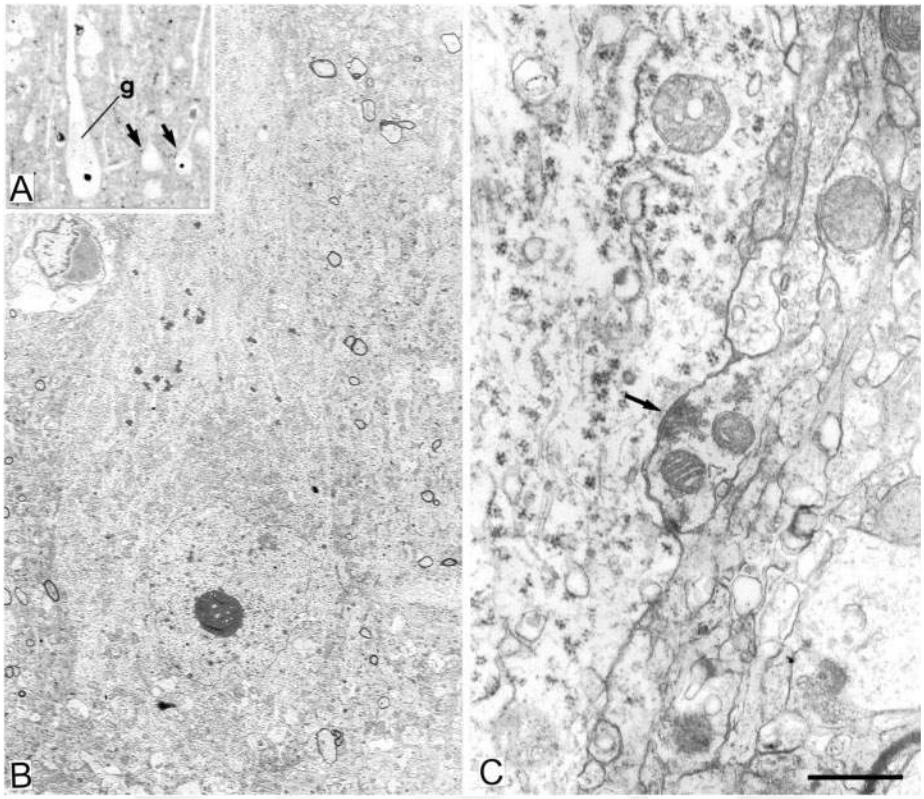

Fig. 8 (**A**) Photomicrograph of a 2 μm thick, semi-thin plastic section counterstained with toluidine blue showing a giant pyramidal cell (g) in the neocortex from patient Mun36. Arrows indicate normal sized pyramidal neurons. (**B**) Low-power electron micrograph taken after resection of the semi-thin section shown in **A**. The perykarion of the giant cell shows a normal complement of organelles. (**C**) Higher magnification of the giant cell to illustrate an axo-somatic symmetrical synapse (arrow). Note the normal looking neuropil around the giant cell. Scale bar (in **C**) 70 μm in **A**, 6.5 μm in **B** and 0.5 μm in **C**.

giant cells. We further studied the perisomatic innervation of these giant neurons in sections adjacent to those studied by immunocytochemistry (Fig. 9D and E) and found them to be surrounded by numerous perisomatic boutons forming conventional symmetrical synapses (Fig. 9G and F). Thus, hypertrophic basket formations made multiple synapses with the neurons they surrounded. While there were few organelles in some perisomatic axon terminals (Fig. 9F), some of them were frequently very large and contained the organelles typical of such structures (i.e. mitochondria and numerous synaptic vesicles; Fig. 9G).

Quantitative electron microscopy

A quantitative electron microscope study was performed at different depths from the pial surface in control neocortical tissue (Table 2) from epileptic patients with hippocampal sclerosis, and in the tissue from epileptic patients with cortical dysplasia (Tables 3–5). Since the laminar boundaries frequently were difficult to distinguish in the dysplastic tissue, three regions of the neocortex were defined in all cases: superficial (0–250 μm from the pial surface), middle (250–550 μm) and deep (550–900 μm), which approximately correspond to layers I, II and III, respectively. In each of these regions, we estimated the synaptic density and proportion of different types of synapses.

The synaptic density varied between different regions of a given patient with cortical dysplasia, as well as between different patients (Table 3). For example, in case Mun34, the synaptic density in the most superficial layer was very low (3420×10^5 synapses/mm^3) in comparison with the deeper layers ($5800–6000 \times 10^5$ synapses mm^3 in the middle and deep parts of the neocortex). In the other two cases (patients H175 and Mun36), we also compared the synaptic density between the normal-looking and the altered regions of tissue from the same patient. In the altered regions of the tissue from patient Mun36, a general decrease in the synaptic density was observed in all layers. In contrast, patient H175 showed a reduction in the synaptic density only in the deeper parts of the altered tissue.

Comparison between synaptic density and neuronal density

Since the neuronal density of different layers and subjects may differ, it is difficult to interpret the differences in the synaptic density in terms of connectivity. Therefore, to study the relationship between the changes in synaptic density

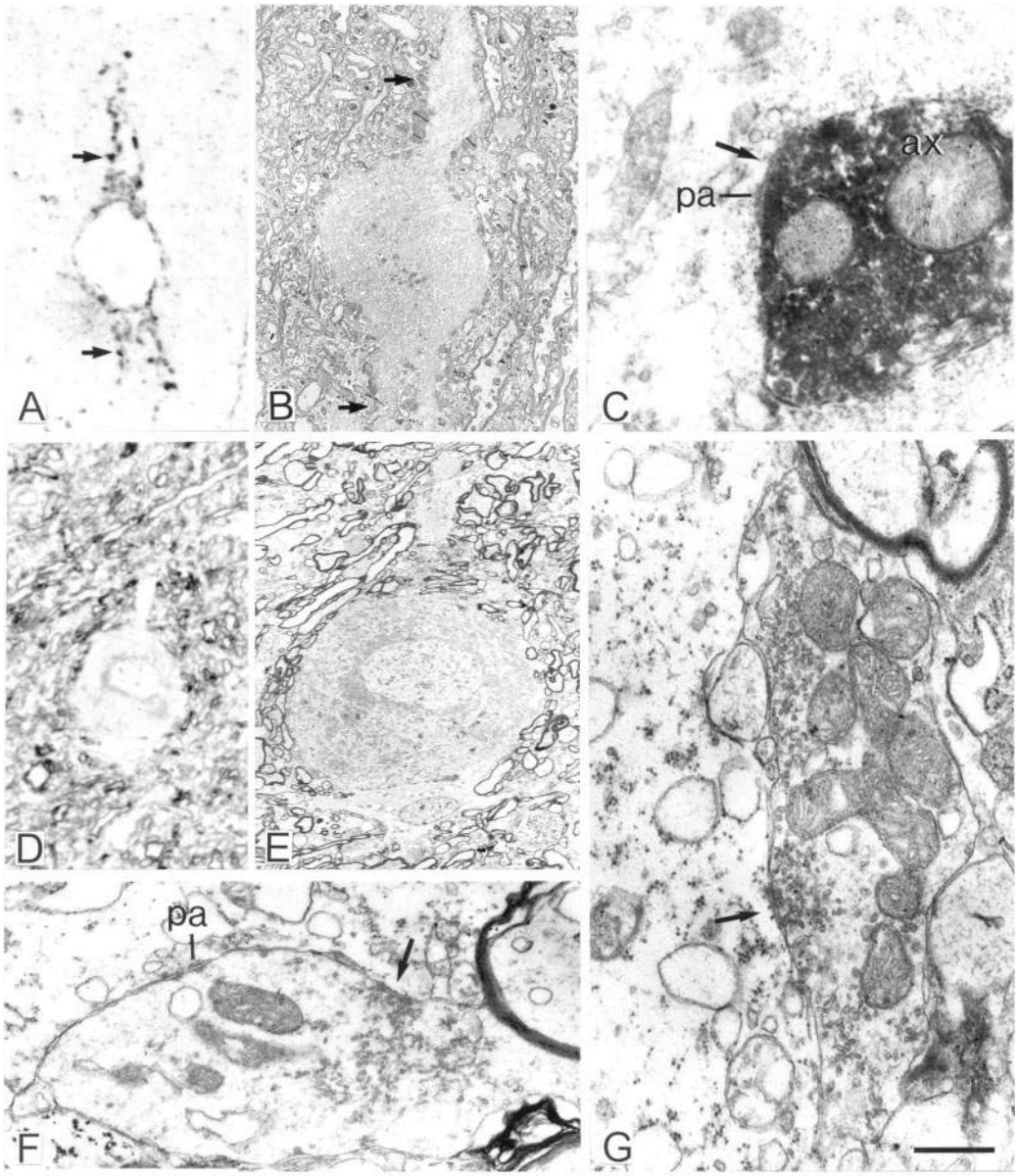

Fig. 9 (**A**–**C**) Correlative light and electron microscope photomicrographs of a hypertrophic basket formation around a giant cell in the white matter. (**A**) Photomicrograph of a 2 μm thick semi-thin plastic section showing the PV-immunoreactive hypertrophic basket formation. Arrows indicate some PV-immunoreactive boutons that make up the basket formations. (**B**) Low-power electron micrograph taken after resection of the semi-thin section shown in **A**. Arrows indicate the same perisomatic PV-immunoreactive boutons as in **A**. (**C**) Higher magnification to illustrate a PV-immunoreactive axon terminal (ax) forming a symmetrical contact (arrow). (**D**–**G**) Correlative light and electron microscope photomicrographs of a giant cell in the white matter. (**D**) Photomicrograph of a 2 μm thick semi-thin plastic section, showing a giant cell. (**E**) Low-power electron micrograph taken after resection of the semi-thin section shown in **D**. (**F** and **G**) Higher magnification to illustrate two axon terminals forming symmetrical synapses (arrows) with the giant neuron. The axon terminal shown in **F** contains relatively few organelles, whereas that shown in **G** is full of organelles. Note the large size of both axon terminals. pa = punctum adherens. Scale bar (in **G**) 30 μm in **A** and **D**, 10 μm in **B** and **E**, 0.35 μm in **C** and **G**, and 0.5 μm in **F**.

and neuronal loss, we calculated the number of synapses per neuron in all the cortical regions and subjects studied (Tables 2 and 5).

In the two cases where the resected tissue included normal-looking cortical regions adjacent to those showing dysplasia (Mun36 and H175), it was particularly relevant to study the alterations in cortical circuits. In these cases, we could compare between the two regions irrespective of the clinical history, age and cortical regions examined. Indeed, the changes in these two patients followed different patterns. In the case of Mun36, there was a reduction in the number of neurons at all depths of the altered region when compared with the normal-looking region (Table 4). This decrease was particularly notable in the middle and deeper portions where

Table 2 *Neuronal density per volume expressed as number of neurons per mm^3 (mean ± SEM), synaptic density per volume expressed as number of synapses × 10^8/mm^3 (mean ± SEM), percentage of synapses and number of synapses per neuron from control tissue*

Case	Distance from pial surface (μm)	Neuronal density	Type of synapse	Synaptic density	Percentage of synapses	Synapses per neuron
H38	0–250 (layer I)	6250 ± 2303	AS	4.35 ± 0.55	89	110 231
			SS	0.56 ± 0.23	11	13 906
			All	10.05 ± 1.49		124 138
	250–550 (layer II)	49 435 ± 5131	AS	4.95 ± 0.58	94	17 574
			SS	0.46 ± 0.19	6	1340
			All	12.11 ± 1.62		18 915
	550–900 (layer III)	18 097 ± 3793	AS	4.69 ± 0.66	89	45 746
			SS	0.72 ± 0.32	11	5684
			All	11.83 ± 1.61		51 431
H60	0–250 (layer I)	9375 ± 2884	AS	8.13 + 1.19	84	137 867
			SS	1.66 ± 0.49	16	27 139
			All	20.04 ± 2.36		165 006
	250–550 (layer II)	44 880 ± 4146	AS	7.49 ± 1.17	99	26 638
			SS	0.22 ± 0.22	1	517
			All	15.79 ± 2.58		27 156
	550–900 (layer III)	18 285 ± 3891	AS	7.01 ± 1.17	90	65 935
			SS	1.00 ± 0.23	10	9209
			All	15.18 ± 2.24		75 144
H94	0–250 (layer I)	9375 ± 2884	AS	1.87 ± 0.35	66	45 138
			SS	1.33 ± 0.28	34	26 248
			All	8.67 ± 1.3		71 386
	250–550 (layer II)	42 373 ± 6420	AS	1.95 ± 0.29	65	7955
			SS	1.35 ± 0.34	35	4835
			All	7.02 ± 1.34		12 790
	550–900 (layer III)	17 700 ± 4135	AS	3.84 ± 0.57	86	37 972
			SS	0.63 ± 0.21	14	5885
			All	9.82 ± 1.46		43 857

Values of the number of synapses per neuron were obtained by dividing the density of the synapses by the density of the neurons after correcting for tissue shrinkage (32.8%). Uncharacterized synapses were included in the asymmetrical and symmetrical types, according to the frequency of both types of synapses in each layer. AS = asymmetrical synapses; SS = symmetrical synapses; All = includes asymmetrical, symmetrical and uncharacterized synapses.

Table 3 *Synaptic density per volume expressed as number of synapses ×10^8/mm^3 (mean ± SEM), and percentage of asymmetrical and symmetrical synapses (in parentheses) per each neocortical region studied in the dysplastic neocortex*

Distance from pial surface (μm)	Type of synapse	H175 normal-looking	H175 dysplastic	Mun36 normal-looking	Mun36 dysplastic	Mun34 dysplastic
0–250 (layer I)	AS	4.12 ± 0.7 (81)	4.96 ± 0.9 (89)	3.33 ± 0.4 (61)	2.40 ± 0.5 (86)	2.42 ± 0.5 (100)
	SS	1.00 ± 0.5 (19)	0.97 ± 0.5 (11)	2.49 ± 0.7 (39)	0.43 ± 0.2 (14)	0.00 ± 0.0 (0)
	All	6.83 ± 0.66	6.79 ± 1.08	11.72 ± 0.83	4.83 ± 0.64	3.42 ± 0.82
250–550 (layer II)	AS	6.43 ± 1.1 (91)	4.80 ± 0.7 (82)	5.98 ± 1.1 (80)	1.84 ± 0.4 (89)	3.18 ± 0.5 (81)
	SS	0.86 ± 0.3 (9)	1.72 ± 0.6 (18)	1.92 ± 0.8 (20)	0.31 ± 0.2 (11)	0.87 ± 0.2 (19)
	All	9.09 ± 1.36	9.14 ± 1.04	18.92 ± 1.17	4.82 ± 0.83	5.8 ± 0.9
550–900 (layer III)	AS	8.46 ± 1.1 (89)	5.11 ± 0.6 (98)	5.05 ± 0.78 (83)	3.46 ± 1.0 (90)	4.37 ± 0.7 (90)
	SS	1.50 ± 0.7 (11)	0.12 ± 0.1 (2)	1.15 ± 0.4 (17)	0.69 ± 0.4 (10)	0.65 ± 0.4 (10)
	All	12.82 ± 1.18	7.06 ± 0.79	15.09 ± 1.99	5.7 ± 1.0	6 ± 0.97

AS = asymmetrical synapses; SS = symmetrical synapses; All = includes asymmetrical, symmetrical and uncharacterized synapses.

a dramatic decrease was observed (49 and 62%, respectively). In contrast, a severe reduction in the number of neurons was only observed in the superficial and deeper portions in case H175 (Table 4). The relationship between the changes in synaptic density and neuronal loss is shown in Table 5. While an increase in this ratio was evident in the superficial part of the altered cortex (65%) in patient H175, in the deeper part of the altered cortex this ratio decreased (23%). Moreover, these changes affected both asymmetrical and symmetrical synapses. In contrast, most of the changes in case Mun36 involved a decrease in the number of synapses/per neuron in the superficial (44%) and middle (50%) layers.

Table 4 *Number of neurons/mm^3 (mean ± SEM) in each neocortical region studied and the percentage change in the number of neurons in the dysplastic regions*

Distance from pial surface (μm)	H175 normal-looking	H175 dysplastic	Mun36 normal-looking	Mun36 dysplastic
0–250 (layer I)	6250 ± 2209	3750 ± 1362, ↓40%	4375 ± 1432	3750 ± 1362, ↓14%
250–550 (layer II)	15 625 ± 2209	16 875 ± 1786, ↑8%	28 125 ± 2017	14 375 ± 2373, ↓49%
550–900 (layer III)	18 750 ± 2209	13 125 ± 2500, ↓30%	29 375 ± 1875	11 250 ± 2119, ↓62%

↓ and ↑ indicate a decrease and increase, respectively.

Table 5 *Number of synapses per neuron*

Distance from pial surface (μm)	Type of synapse	H175 normal-looking	H175 dysplastic	Mun36 normal-looking	Mun36 dysplastic
0–250 (layer I)	AS	68 384	118 133, ↑73%	125 029	85 600, ↓32%
	SS	16 460	21 867, ↑33%	86 171	14 667, ↓83%
	All	84 844	140 000, ↑65%	211 200	100 267, ↓53%
250–550 (layer II)	AS	39 680	32 296, ↓19%	41 244	23 026, ↓44%
	SS	4992	10 015, ↑101%	11 556	3270, ↓72%
	All	44 672	42 311, ↓5%	52 800	26 296, ↓50%
550–900 (layer III)	AS	46 453	40 533, ↓13%	32 817	34 578, ↑5%
	SS	7573	914, ↓88%	7013	5867, ↓16%
	All	54 027	41 448, ↓23%	39 830	40 444, ↑2%

Values were obtained by dividing the density of the synapses by the density of the neurons after correcting for tissue shrinkage (32.8%). Uncharacterized synapses were included in the asymmetrical and symmetrical types, according to the frequency of both types of synapses in each layer. AS = asymmetrical synapses; SS = symmetrical synapses; All = includes asymmetrical, symmetrical and uncharacterized synapses. ↓ and ↑ indicate a decrease and increase, respectively.

These changes affected both asymmetrical and especially symmetrical synapses.

Discussion

We have analysed the neocortex in tissue removed from epileptic patients suffering from FCD with the aim of identifying alterations that may be implicated in the development of seizures. Our main conclusion from these studies is that this tissue shows a remarkable variety of alterations in the GABAergic system, both between patients and between different regions within a given patient. Moreover, the density of excitatory and inhibitory synapses per volume in the dysplastic cortex was different from that of the normal cortex that was adjacent to it. These modifications included increases or reductions in synaptic density, and changes in the proportion of excitatory and inhibitory synapses.

Histopathological findings

The histopathological alterations observed in the tissue analysed here were similar to those found in previous reports, including the disruption of the cortical laminae and the cytological abnormalities, such as the presence of balloon cells, and of giant and dysmorphic neurons (for a review see Tassi *et al*., 2002). Balloon cells contain cytoskeletal components such as vimentin and glial fibrillary acidic protein (Garbelli *et al*., 1999*a*), which indicates that these cells may be of glial origin. Indeed, electrophysiological studies of these cells have shown absence of voltage- and ligand-gated currents, as well as an apparent lack of spontaneous synaptic inputs (Cepeda *et al*., 2003). Moreover, the ultrastructural analysis of balloon cells that we performed revealed that these cells do not establish synaptic contacts. Thus, these anatomical findings confirm the lack of functional synapses on balloon cells described by Cepeda *et al*. (2003), and support the idea that they are of a non-neuronal origin.

Indeed, the absence of synaptic contacts suggests that these cells are not directly involved in the origin or the propagation of epileptogenic activity (but see Cepeda *et al*., 2003). In contrast, the giant pyramidal cells that we analysed had what appeared to be a normal complement of organelles, and their somata and proximal dendrites establish conventional symmetrical synapses (see below).

Immunocytochemical studies

As has been demonstrated previously, changes in the expression of GABAergic markers, such as decreases in the levels of PV immunoreactivity, were detected in the neocortex of FCD tissue (Spreafico *et al*., 1998*a*, *b*; Garbelli *et al.*, 1999*a*, *b*). GABA is the main inhibitory neurotransmitter in the brain and, therefore, a reduction in the activity of the GABAergic system could make the dysplastic tissue more susceptible to sudden and prolonged hyperexcitability (Crino *et al*., 2001). In the primate neocortex, different types of GABAergic interneurons innervate pyramidal cells. Among these interneurons,

chandelier and basket cells are considered to be the strongest inhibitory neurons and both contain PV (reviewed in DeFelipe, 1999). In the present work, we confirm and extend previous studies performed in cortical dysplastic tissues (Garbelli *et al*., 1999*a*), showing that the changes in the PV distribution were not homogeneous throughout the lesioned neocortex, either in tissue from the same patient or between patients. For example, in certain regions, there was a remarkable decrease in PV-immunoreactive chandelier terminals, suggesting a modification of the GABAergic system that would profoundly affect the inhibitory control of pyramidal cells (DeFelipe, 1999). However, we also found increases in PV immunoreactivity or the aberrant expression of PV in axons within other regions of the FCD tissue. The most striking change of this type was the presence of hypertrophic basket formations in the white matter (see also Ferrer *et al*., 1994; Spreafico *et al*., 1998*a*; Garbelli *et al*., 1999*a*).

Basket formations in the white matter

Hypertrophic PV-immunoreactive basket formations were found around the ectopic giant neurons in the white matter, establishing symmetrical synapses. Several lines of evidence indicate that in the primate neocortex, PV-immunoreactive terminals forming asymmetrical synapses arise from thalamocortical afferent fibres, while those forming symmetrical synapses arise from intrinsic GABAergic neurons (DeFelipe and Jones, 1991; del Río and DeFelipe, 1994). Since PV-immunoreactive somata were not present in the white matter, it seems most likely that these basket formations originate from basket cells located in the grey matter whose axons have sprouted as a consequence of the changes induced by the malformations or the epileptic state. Previous electron microscope studies of hypertrophic PV-immunoreactive basket formations showed few synaptic contacts between these boutons and the somata of innervated cells (Garbelli *et al*., 1999*a*). Similarly, we found few axosomatic PV-immunoreactive synaptic contacts from basket formations in our preparations. Nevertheless, it was often difficult to discern synaptic contacts because of the intense immunostaining that masked the synaptic membrane specializations. Therefore, we studied the perisomatic boutons around giant cells by conventional electron microscopy. We found that neurons in the white matter received multiple symmetrical (inhibitory) synapses, indicating that hypertrophic basket formations do form conventional synaptic contacts. However, perisomatic boutons were hypertrophic while those found around the giant pyramidal cells in the grey matter were of a normal size. This suggests that the basket formations in the white matter originate from particular types of basket cells that have sprouted.

Interestingly, similar hypertrophic basket formations have been described recently in the sclerotic epileptic hippocampus (Arellano *et al*., 2004), and it is possible that both these hypertrophic basket formations may originate through a common mechanism. For example, in both cases, the changes observed in the GABAergic system might be secondary to epilepsy, which induces synaptic plasticity and axonal reorganization, or due to a defect in cortical development (see Blümcke *et al*., 2002; Arellano *et al*., 2004). Since hypertrophic basket formations in FCD were immediately adjacent to the regions where the distribution of PV was normal, it seems likely that these alterations were not due to epileptic activity *per se* because the adjacent regions should be equally affected. Interestingly, in the grey matter just above the region where the giant cells were located in the white matter, there was a clear reduction in the number of chandelier terminals. Furthermore, in the regions of the grey matter showing hypertrophic basket formations, chandelier terminals were absent or very scarce. The increase of axo-somatic innervation on the one hand, and the decrease of axo-axonic innervation on the other, suggests that this may represent a compensatory mechanism that enhances the inhibition of hyperexcitable pyramidal cells.

Synaptic density in the neuropil

Several electrophysiological studies have shown that ictal discharges can be generated in slices from FCD tissue, suggesting the existence of an imbalance between excitatory and inhibitory circuits (Mattia *et al*., 1995; Avoli *et al*., 1999, 2003; Mathern *et al*., 2000; Lurton *et al*., 2002). This is in line with the dramatic changes we observed in synaptic density and in the proportion of excitatory and inhibitory synapses in the neuropil, where the majority of synapses are located (reviewed in DeFelipe and Fariñas, 1992). Since neuronal loss was more prominent in some cortical regions than in others, we examined the relationship between the changes in synaptic density and neuronal loss. We found distinct changes in the number of synapses per neuron, which affected both asymmetrical and symmetrical synapses and that were not correlated with the degree of neuronal loss. These observations indicate that there is an imbalance between excitatory and inhibitory systems, which is most likely to have important functional implications. The fact that the alterations were not homogeneous between different regions within a given patient or between patients suggests that these alterations are rather complex and that they affect a large variety of cortical circuits. In addition, some of the alterations might be related to epilepsy whereas others may not. For example, in the tissue from patient Mun36, there were some cortical regions that seem unlikely to contribute to epileptiform activity since there was intense gliosis, few neurons and virtually no synapses. However, other regions could potentially contribute to the hyperexcitability since they contained numerous neurons and synapses, and the GABAergic circuits appeared to be abnormal due to the reduced number of chandelier cells. Furthermore, alterations occurred at different depths from the pial surface. This is also important because neurons located in different layers are involved in different circuits, in terms of both their afferent and efferent connections

(e.g. White, 1989). Indeed, in layer I from patient Mun34, all the synapses were asymmetrical, indicating that inhibitory circuits are absent or highly reduced, and suggesting that this layer may be hyperexcitable in this particular case.

In conclusion, several kinds of alterations may underlie the hyperexcitability of FCD tissue, although it remains unclear which may be the consequence of the malformations and which may be a result of epileptic activity *per se*. Moreover, it also remains a possibility that some of these changes are the product of a compensatory plastic mechanism to avoid epilepsy. Further electrophysiological studies, in conjunction with correlative microanatomical and neurochemical characterization of the dysplastic tissue, will be necessary to define the functional significance of specific changes in the neocortical circuits of these epileptic patients.

Caveats

There are six limitations that should be highlighted in the present study. (i) All of our data regarding epileptic patients were derived from only three cases with cortical dysplasia, precluding the extrapolation of the results to the whole population of epileptic patients with this pathology. Rather, our results emphasize the complex alterations in cortical circuits that occur in these patients. (ii) It has been shown in animal models of epilepsy that seizure activity may reduce PV immunolabelling (e.g. Sloviter, 1989). Therefore, the variability of PV staining in the three patients could be explained in part by the individual's history of seizure activity (frequency, intensity and duration of seizures). (iii) One patient was seizure free, but the other two patients continued to suffer seizures. However, the sites sampled for electron microscopy may not represent the regions of seizure onset in the latter two patients. Nevertheless, both these patients with post-surgical seizures showed a worthwhile improvement, which might indicate that the resected tissue was indeed epileptogenic but that a residual area of epileptogenic cortex was not surgically resected. (iv) Possible changes in synaptic density as a function of age (e.g. Rakic *et al*., 1994), or due to the effects of anti-epileptic drugs or those of repeated seizures on synaptic density preclude comparing between patients of different ages and with different clinical histories. Nevertheless, the effects of anti-epileptic drugs can be ruled out because control neocortical tissue was obtained from epileptic patients with hippocampal sclerosis that were being treated with drugs similar to the dysplastic patients. Thus, differences in the synaptic circuits between control and dysplastic tissue may be interpreted as the result of the pathological changes produced by the focal cortical dysplasia. (v) At the electron microscope level, not all synapses can be classified as asymmetrical (putative excitatory) or symmetrical (putative inhibitory) because the synaptic cleft and associated membrane densities cannot be clearly visualized in a number of synapses due to the oblique plane of section (e.g. DeFelipe *et al*., 1999). In this study, these uncharacterized synapses were included as asymmetrical and symmetrical types, according to the frequency of both types of synapses. Therefore, the proportion of each type of synapse in this work is an estimation of the real ratio. (vi) Samples of the neocortex from epileptic patients with hippocampal sclerosis were used as controls. These neocortical samples were considered to be normal, based on intraoperative electrocorticography, routine histopathological examination and other immunocytochemical studies performed on the resected tissue. Nevertheless, this material comes from patients with chronic seizures, and therefore we could not compare our results with true control specimens.

Acknowledgements

We wish to thank A. Ortiz for technical assistance, C. Hernandez for assistance with the confocal microscope, J. A. Maldonado for assistance with the electron microscope, M. C. Gonzalez-Albo for her earlier contribution to this project, and Dr G. Lo Russo ('Claudio Munari' Epilepsy Surgery Center of Niguarda Hospital, Milano) for supplying human tissue. The following institutions have supported this work: Spanish Ministry of Education and Science (grant PM99-0105, BFI2003-02745 and a research fellowship for L.A.-N., FP2000-4989), Comunidad de Madrid (grant 08.5/0027/2001) and the Italian Ministry of Health and FIRB (grant RBNEOINR34-008).

References

Alonso-Nanclares L, White EL, Elston GN, DeFelipe J. Synaptology of the proximal segment of pyramidal cell basal dendrites. Eur J Neurosci 2004; 19: 771–6.

Arellano JI, Munoz A, Ballesteros-Yanez I, Sola RG, DeFelipe J. Histopathology and reorganization of chandelier cells in the human epileptic sclerotic hippocampus. Brain 2004; 127: 45–64.

Avoli M, Bernasconi A, Mattia D, Olivier A, Hwa GG. Epileptiform discharges in the human dysplastic neocortex: in vitro physiology and pharmacology. Ann Neurol 1999; 46: 816–26.

Avoli M, Louvel J, Mattia D, Olivier A, Esposito V, Pumain R, et al. Epileptiform synchronization in the human dysplastic cortex. Epileptic Disord 2003; 5 Suppl 2: S45–50.

Babb TL, Ying Z, Mikuni N, Nishiyama K, Drazba J, Bingaman W, et al. Brain plasticity and cellular mechanisms of epileptogenesis in human and experimental cortical dysplasia. Epilepsia 2000; 41 Suppl 6: S76–81.

Blümcke I, Thom M, Wiestler OD. Ammon's horn sclerosis: a maldevelopmental disorder associated with temporal lobe epilepsy. Brain Pathol 2002; 12: 199–211.

Cepeda C, Hurst RS, Flores-Hernandez J, Hernandez-Echeagaray E, Klapstein GJ, Boylan MK, et al. Morphological and electrophysiological characterization of abnormal cell types in pediatric cortical dysplasia. J Neurosci Res 2003; 72: 472–86.

Colonnier M. Synaptic patterns on different cell types in the different laminae of the cat visual cortex. An electron microscope study. Brain Res 1968; 9: 268–87.

Colonnier M. The electron microscopic analysis of the neuronal organization of the cerebral cortex. In: Schmitt FO, Worden FG, Adelman G, Dennis SG, editors. Organization of the cerebral cortex. Cambridge (MA): MIT Press; 1981. p. 125–52.

Crino PB, Duhaime AC, Baltuch G, White R. Differential expression of glutamate and GABA-A receptor subunit mRNA in cortical dysplasia. Neurology 2001; 56: 906–13.

DeFelipe J. Chandelier cells and epilepsy. Brain 1999; 122: 1807–22.

DeFelipe J, Farinas I. The pyramidal neuron of the cerebral cortex: morphological and chemical characteristics of the synaptic inputs. Prog Neurobiol 1992; 39: 563–607.

DeFelipe J, Fairén A. A simple and reliable method for correlative light and electron microscopic studies. J Histochem Cytochem 1993; 41: 769–72.

DeFelipe J, Jones EG. Parvalbumin immunoreactivity reveals layer IV of monkey cerebral cortex as a mosaic of microzones of thalamic afferent terminations. Brain Res 1991; 562: 39–47.

DeFelipe J, Hendry SH, Jones EG. Visualization of chandelier cell axons by parvalbumin immunoreactivity in monkey cerebral cortex. Proc Natl Acad Sci USA 1989; 86: 2093–7.

DeFelipe J, Garcia SR, Marco P, Del Rio MR, Pulido P, Cajal S. Selective changes in the microorganization of the human epileptogenic neocortex revealed by parvalbumin immunoreactivity. Cereb Cortex 1993; 3: 39–48.

DeFelipe J, Marco P, Busturia I, Merchan-Perez A. Estimation of the number of synapses in the cerebral cortex: methodological considerations. Cereb Cortex 1999; 9: 722–32.

DeFelipe J, Alonso-Nanclares L, Arellano JI. Microstructure of the neocortex: comparative aspects. J Neurocytol 2002; 31: 299–316.

del Rio MR, DeFelipe J. A study of SMI 32-stained pyramidal cells, parvalbumin-immunoreactive chandelier cells, and presumptive thalamocortical axons in the human temporal neocortex. J Comp Neurol 1994; 342: 389–408.

Engell JJ. Outcome with respect to epileptic seizures. In: Engell JJ, editor. Surgical treatment of epilepsies. New York: Raven Press, 1987: 553–71.

Feldman ML. Morphology of the neocortical pyramidal neuron. In: Jones EG, Peters A, editors. Cerebral cortex. New York: Plenum Press; 1984. p. 123–200.

Ferrer I, Oliver B, Russi A, Casas R, Rivera R. Parvalbumin and calbindin-D28k immunocytochemistry in human neocortical epileptic foci. J Neurol Sci 1994; 123: 18–25.

Garbelli R, Munari C, De Biasi S, Vitellaro-Zuccarello L, Galli C, Bramerio M, et al. Taylor's cortical dysplasia: a confocal and ultrastructural immunohistochemical study. Brain Pathol 1999a; 9: 445–61.

Garbelli R, Pasquier B, Minotti L, Tassi L, De Biasi S, Benabid AL, et al. Inmunocytochemical studies in epileptogenic dysplastic tissue. In: Spreafico R, Avanzini G, Andermann F, editors. Abnormal cortical development and epilepsy. John Libbey; 1999b. p. 241–50.

Gray EG. Electron microscopy of synaptic contacts on dendrite spines of the cerebral cortex. Nature 1959; 183: 1592–3.

Hendry SH, Jones EG, Emson PC, Lawson DE, Heizmann CW, Streit P. Two classes of cortical GABA neurons defined by differential calcium binding protein immunoreactivities. Exp Brain Res 1989; 76: 467–72.

Honavar M, Meldrum BS. Epilepsy. In: Graham DI, Lantos PL, editors. Greenfield's neuropathology. 6th edn. London: Arnold; 1997. p. 931–71.

Kerfoot C, Vinters HV, Mathern GW. Cerebral cortical dysplasia: giant neurons show potential for increased excitation and axonal plasticity. Dev Neurosci 1999; 21: 260–70.

Kuzniecky RI, Barkovich AJ. Pathogenesis and pathology of focal malformations of cortical development and epilepsy. J Clin Neurophysiol 1996; 13: 468–80.

Lurton D, Yacubian EM, Sanabria EG, da Silva AV, Vianna R, Garzon E, et al. Immunohistochemical study of six cases of Taylor's type focal cortical dysplasia: correlation with electroclinical data. Epilepsia 2002; 43 Suppl 5: S217–9.

Marco P, DeFelipe J. Altered synaptic circuitry in the human temporal neocortex removed from epileptic patients. Exp Brain Res 1997; 114: 1–10.

Mathern GW, Cepeda C, Hurst RS, Flores-Hernandez J, Mendoza D, Levine MS. Neurons recorded from pediatric epilepsy surgery patients with cortical dysplasia. Epilepsia 2000; 41 Suppl 6: S162–7.

Mattia D, Olivier A, Avoli M. Seizure-like discharges recorded in human dysplastic neocortex maintained *in vitro*. Neurology 1995; 45: 1391–5.

Meldrum BS, Bruton CJ. Epilepsy. In: Adams J, Duchen LW, editors. Greenfield's neuropathology. 5th edn. London: Arnold; 1992. p. 1246–83.

Palmini A, Gambardella A, Andermann F, Dubeau F, da Costa JC, Olivier A, et al. Operative strategies for patients with cortical dysplastic lesions and intractable epilepsy. Epilepsia 1994; 35 Suppl 6: S57–71.

Peachey LD. Thin sections. I. A study of section thickness and physical distortion produced during microtomy. J Biophys Biochem Cytol 1958; 4: 233–42.

Peters A. Synaptic specificity in the cerebral cortex. In: Edelman GM, Gall WE, Cowan WM, editors. Synaptic function. New York: John Wiley; 1987. p. 373–97.

Peters A, Palay SL. The morphology of synapses. J Neurocytol 1996; 25: 687–700.

Peters A, Palay SL, Webster HD. The fine structure of the nervous system. Neurons and their supporting cells. New York: Oxford University Press; 1991.

Prayson RA, Spreafico R, Vinters HV. Pathologic characteristics of the cortical dysplasias. Neurosurg Clin North Am 2002; 13: 17–25.

Rakic P, Bourgeois J-P, Goldman-Rakic PS. Synaptic development of the cerebral cortex: implications for learning, memory, and mental illness. Prog Brain Res 1994; 104: 227–43.

Ribak CE, Roberts RC. GABAergic synapses in the brain identified with antisera to GABA and its synthesizing enzyme, glutamate decarboxylase. J Electron Microsc Tech 1990; 15: 34–48.

Sloviter RS. Calcium binding protein (calbindin-D28K) and parvalbumin immunocytochemistry: localization in the rat hippocampus with specific reference to the selective vulnerability of hippocampal neurons to seizure activity. J Comp Neurol 1989; 280: 183–96.

Spreafico R, Battaglia G, Arcelli P, Andermann F, Dubeau F, Palmini A, et al. Cortical dysplasia: an immunocytochemical study of three patients. Neurology 1998a; 50: 27–36.

Spreafico R, Pasquier B, Minotti L, Garbelli R, Kahane P, Grand S, et al. Immunocytochemical investigation on dysplastic human tissue from epileptic patients. Epilepsy Res 1998b; 32: 34–48.

Spreafico R, Tassi L, Colombo N, Bramerio M, Galli C, Garbelli R, et al. Inhibitory circuits in human dysplastic tissue. Epilepsia 2000; 41 Suppl 6: S168–73.

Tassi L, Colombo N, Garbelli R, Francione S, Lo RG, Mai R, et al. Focal cortical dysplasia: neuropathological subtypes, EEG, neuroimaging and surgical outcome. Brain 2002; 125: 1719–32.

Taylor DC, Falconer MA, Bruton CJ, Corsellis JA. Focal dysplasia of the cerebral cortex in epilepsy. J Neurol Neurosurg Psychiatry 1971; 34: 369–87.

West MJ, Gundersen HJ. Unbiased stereological estimation of the number of neurons in the human hippocampus. J Comp Neurol 1990; 296: 1–22.

White EL. Cortical circuits: synaptic organization of the cerebral cortex. Boston: Birkhäuser; 1989.

Williams RW, Rakic P. Three-dimensional counting: an accurate and direct method to estimate number of cells in sectioned material. J Comp Neurol 1988; 278: 344–52.

Ying Z, Babb TL, Comair YG, Bingaman W, Bushey M, Touhalisky K. Induced expression of NMDAR2 proteins and differential expression of NMDAR1 splice variants in dysplastic neurons of human epileptic neocortex. J Neuropathol Exp Neurol 1998; 57: 47–62.